Proposal for J-PARC 50 GeV Proton Synchrotron

Study of isospin dependence of kaon-nucleus interaction by in-flight ^{3}He($K^-, n/p$) reactions

H. Fujioka* (Spokesperson), T. Hiraiwa, T. Nagae, Y. Sada
Kyoto University, Japan

S. Ishimoto, M. Iwai, M. Sekimoto, S. Suzuki, A. Toyoda
High Energy Accelerator Research Organization (KEK), Japan

D. Faso, O. Morra
INFN Sez. di Torino, Italy

C. Curceanu, C. Guaraldo, S. Okada, A. Romero Vidal, D. Sirghi, F. Sirghi, O. Vazquez Doce
Laboratori Nazionali di Frascati dell'INFN, Italy

T. Fukuda, Y. Mizoi
Osaka Electro-Communication University, Japan

A. Sakaguchi
Osaka University, Japan

S. Ajimura, S. Enomoto, H. Noumi
Research Center for Nuclear Physics (RCNP), Osaka University, Japan

M. Iio, K. Itahashi, M. Iwasaki, H. Ohnishi, H. Outa, F. Sakuma, D. Tomono, K. Tsukada, T. Yamazaki
RIKEN Nishina Center, RIKEN, Japan

P. Bühler, M. Cargnelli, T. Ishiwatari, J. Marton, K. Suzuki, E. Widmann, J. Zmeskal
Stefan Meyer Institute for Subatomic Physics, Austria

H. Bhang, S. Choi, H. Yim
Seoul National University, South Korea

*e-mail: fujioka@scphys.kyoto-u.ac.jp

Y. Fukuda, M. Tokuda
Tokyo Institute of Technology, Japan

J. Chiba, T. Hanaki
Tokyo University of Science, Japan

P. Kienle
Technische Universität München, Germany

L. Busso
Università di Torino, Italy

Y. Fujiwara, R. S. Hayano, T. Ishikawa, Y. Matsuda, M. Sato, T. Suzuki, H. Tatsuno
University of Tokyo, Japan

G. Beer
University of Victoria, Canada

June 16, 2009

Abstract

We propose to measure the ^{3}He(K^-, p) reaction, in addition to the (K^-, n) reaction which has been already proposed in the E15 experiment. The comparison of the two kinds of missing-mass spectra will provide us unique information on the isospin dependence of the kaon-nucleus ($\overline{K}$–NN) interaction, because they are expected to originate from different isospin configurations.

This measurement will be realized by installing a proton detector system in the present E15 setup without a serious influence to the original measurement of E15, so that both the spectra can be obtained simultaneously.

1 Physics Motivation

Almost half a century has passed after Nogami predicted a possible existence of $\overline{K}NN$ bound states for the first time [1]. His idea was based on the assumption that the $\Lambda(1405)$, which had been already discovered by Alston *et al.* [2], is a $\overline{K}N$ bound state. He concluded that $[\overline{K}(NN)_{T_{NN}=1}]_{T=1/2}$, where T_{NN} and T are the isospin of two nucleons and the total isospin respectively, is most favored among possible isospin configurations.

After significant progress of understanding of $\overline{K}N$ interaction, deduced from kaon-nucleon scattering measurements and kaonic hydrogen data, Akaishi and Yamazaki predicted the existence of a light $\overline{K}$-nuclear bound states [3, 4]. They also regarded the $\Lambda(1405)$ as a $\overline{K}N$ bound state with its binding energy 27 MeV. For example, the binding energy and decay width of the K^-pp system, which is the lightest kaon-nuclear bound state, were calculated to be 48 MeV and 61 MeV, respectively [4, 5].

Motivated by this stimulating prediction, the KEK-PS E471/E549 experiments investigated the ^{4}He($K^-_{\rm stop}$, N) reaction. No narrow peak structure was found in the (K^-, p) reaction, and a tight upper limit of the formation ratio of the K^-pnn state was obtained [6]. For the (K^-, n) reaction, a peak structure, corresponding to the K^-ppn state, was observed in E471 [7]. Analysis of the E549 data is in progress now. Recently, they studied the correlation of hyperon-nucleon (ΛN) [8] or hyperon-deuteron (Λd) [9] from the stopped K^- absorption in ^{4}He. Components which can be hardly explained by two- or three-nucleon absorption have been observed, and it may indicate the existence of strange multibarionic system.

On the other hand, the FINUDA experiment was carried out for the purpose of hypernuclear physics with the stopped K^- reaction at the DAΦNE e^+e^- collider. They observed the correlation of back-to-back Λ and proton from ^{6}Li, ^{7}Li, ^{12}C, prior to the KEK-PS experiments, and they found that their invariant mass distributes far below the $K^- + p + p$ threshold. Hence a possibility of the observation of K^-pp nuclear bound states, decaying into $\Lambda + p$, was suggested [10].

In addition, heavy ion collision experiment by FOPI (GSI) [11], antiproton-^{4}He annihilation experiment by OBELIX (CERN) [12], and proton-proton collision experiment by DISTO (SATURNE) [13] reported signals from kaon-nuclear bound states.

However, the existence of kaon bound states is not confirmed so far, especially because some other interpretations for the observed peak structures might be possible. It is difficult to validate an interpretation to assign an observed peak to a kaon bound state, just only by investigating either *formation* reactions or *decay* reactions. An experiment to measure all the final state particles, i.e. *formation and decay* (so-called a "perfect" experiment) is strongly required for much better understanding of the reaction itself [1]. In addition to the J-PARC E15 experiment [14] which will be explained later, two more experiments are proposed by FOPI (GSI) [15] and AMADEUS (DAΦNE) [16].

Theoretical calculations, especially on the structure of the lightest K^-pp system, have been carried out in a Faddeev calculation [17, 18] and a variational approach [4, 5, 19]. Partially because the $\overline{K}N$ interaction used in the calculations are different from each other, their results are not completely consistent. Nevertheless, all the calculations suggest the K^-pp system will be bound thanks to the existence of $\Lambda(1405)$, and the binding energy will be in the range of 20 to 70 MeV, while the decay width is estimated to be moderately large, from several tens to a hundred MeV. It should be noted that what we observe experimentally may be not kaon-nulear bound states, but Λ^* hypernuclei [20]. We need theoretical help to distinguish them using experimental observables.

By the way, aside from the kaon-nuclear bound states, the kaon-nuclear interaction can be examined in different ways. Although the interaction between an antikaon and a nucleus near threshold is known to be attractive from experimental data on various kinds of kaonic atoms, its strength is not yet to be converged [21]. While the global fit with a density-dependent potential gives as deep a potential at the nuclear center as 150–200 MeV, the fit with a $t\rho$ potential results in a shallower depth around 80 MeV [22–24]. Moreover, an optical potential derived from the chiral unitary model [25], which is further shallower (40–60 MeV), could explain the experimetally

[1] In the analysis of the DISTO experiment [13], both of the formation process $p + p \to K^+ + X$ and the decay process $X \to \Lambda + p$ were investigated simultaneously.

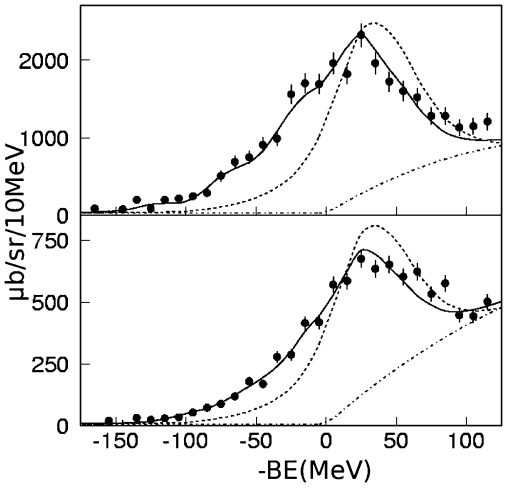

Figure 1: Missing-mass spectra of the ^{12}C(K^-, n) reaction (upper) and the ^{12}C(K^-, p) reaction (lower) obtained by the KEK-PS E548 experiment. The spectra were fitted with theoretically calculated ones with Green's function method (solid lines). Taken from [33].

measured energy shifts and widths [26]. Since the overlapping of K^- and nuclear wavefunctions in a kaonic atom is maximum around the low-density nuclear surface, a large ambiguity remains in the central region of the nucleus.

In order to investigate the strength of the kaon-nucleus interaction, Kishimoto proposed a nuclear reaction (in-flight K^-, N) [27]. Detailed theoretical studies of the formation spectrum can be found in [28–31]. The (K^-, N) reactions for carbon and oxygen targets have been measured in the BNL-AGS E930 [32] and KEK-PS E548 [33] experiments. The missing-mass spectra of the ^{12}C(K^-, n/p) reactions in E548, shown in Fig. 1, indicate a strong attraction between antikaon and nucleus. After fitting with calculated spectra by the Green's function method, the best fit gives the potential depth of ~ 190 MeV for the (K^-, n) reaction and ~ 160 MeV for the (K^-, p) reaction. They attributed the difference between the two reactions to the isospin dependence, i.e. the number of the $I = 0$ $\overline{K}N$ pairs.

Based on the current situation, we proposed the J-PARC E15 experiment [14], which will investigate the ^{3}He(K^-, n)K^-pp reaction with the beam momentum 1.0 GeV/c. Forward scattered neutrons are to be detected by a neutron counter, composed of 112 plastic scintillators (16 segments $\times$ 7 layers), located 15 m downstream of the target. Assuming the time-of-flight resolution to be 120 ps, the missing-mass resolution is estimated to be 20 MeV/c^2 (FWHM). Furthermore, a Λ particle (decaying into $p + \pi^-$) and proton from a non-mesonic decay mode of $K^-pp \to \Lambda + p$ will be detected by a cylindrical detector system (CDS) surrounding the helium-3 target. It enables us the invariant-mass spectroscopy with the resolution 37 MeV/c^2 (FWHM), and all the particles in the final state will be detected.

After the E15 proposal was submitted, Yamagata-Sekihara *et al.* calculated the formation spectra of the ^{3}He(K^-, N) reactions by using the distorted-wave impulse approximation (DWIA) calculation [34], which has been already applied for ^{12}C and ^{16}O targets [31]. The formation of the ^{3}He(K^-, N) reaction was independently investigated by Koike and Harada [35, 36]. In both calculations [34, 35], the strength

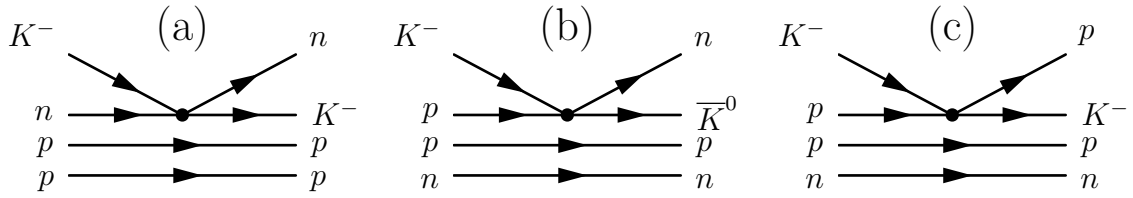

Figure 2: Possible diagrams for ^{3}He(K^-, n) [(a) and (b)] and (K^-, p) [(c)] reactions in the impulse approximation.

function was derived by the Green's function method, developed by Morimatsu and Yazaki [37]. The Green's function was obtained by assuming the optical potential between an antikaon and a two-nucleon system ($\overline{K}$–NN). Yamagata-Sekihara *et al.* obtained an energy-dependent optical potential from the chiral unitary amplitudes T within the $T\rho$ approximation. Koike and Harada investigated the dependence of the spectra shape on the optical potential, parametrized by a Gaussian form as $U_{K^-pp}(r) = (V_0 + iW_0)\exp[-(r/\beta)^2]$, where β is the range parameter (1.09 fm).

In the impulse approximation, the elementary process of the ^{3}He(K^-, N) reaction is $K^- + N \to N + \overline{K}$. Only the elastic reaction $K^- + p \to p + K^-$ can contribute to the (K^-, p) reaction, while both the elastic reaction $K^- + n \to n + K^-$ and the charge-exchange reaction $K^- + p \to n + \overline{K}^0$ can occur in case of the (K^-, n) reaction. The corresponding diagrams are drawn in Fig. 2. The forward differential cross sections for the three reactions at $p_{K^-} = 1.0\,\mathrm{GeV}/c$ are obtained as [36]:

$$\left(\frac{d\sigma}{d\Omega}(0^\circ)\right)_{\mathrm{lab}}^{K^-N\to N\overline{K}} = 24.5\,\mathrm{mb/sr},\ \text{for}\ K^- + n \to n + K^-,$$
$$= 13.1\,\mathrm{mb/sr},\ \text{for}\ K^- + p \to n + \overline{K}^0,$$
$$= 9.4\,\mathrm{mb/sr},\quad \text{for}\ K^- + p \to p + K^-,$$

from the partial wave analysis by Gopal *et al.* [38]

The residual $\overline{K}NN$ system can have three kinds of isospin configurations, such as:

(1) $T = 1/2$ and $T_{NN} = 1$ (total spin: 0)

(2) $T = 1/2$ and $T_{NN} = 0$ (total spin: 1)

(3) $T = 3/2$ and $T_{NN} = 1$ (total spin: 0)

where T and T_{NN} denote the total isospin and the isospin of the NN system, respectively. It should be noted that the total spin is uniquely determined for each configuration, because of the Pauli principle, if the angular momentum of each particle is zero. The K^-pp bound state is expected to have configuration (1) [2], resulting in $J^\pi = 0^-$ [4, 5, 17, 19]. This is because the number of the $\overline{K}N$ pairs with the isospin 0 is maximized in configuration (1). A small mixing with configuration (2) may help to increase the binding energy [19].

[2]If a dibaryonic state with the strangeness -1 is not a kaon-nucleus bound state $\overline{K}NN$, but a two-body Λ^*N bound state, the total isospin and spin may be different from configuration (1). For example, Arai *et al.* showed the $S = 1, I = 1/2$ state could be the ground state, due to the ω-exchange potential (attractive for $S = 1$ and repulsive for $S = 0$) [20].

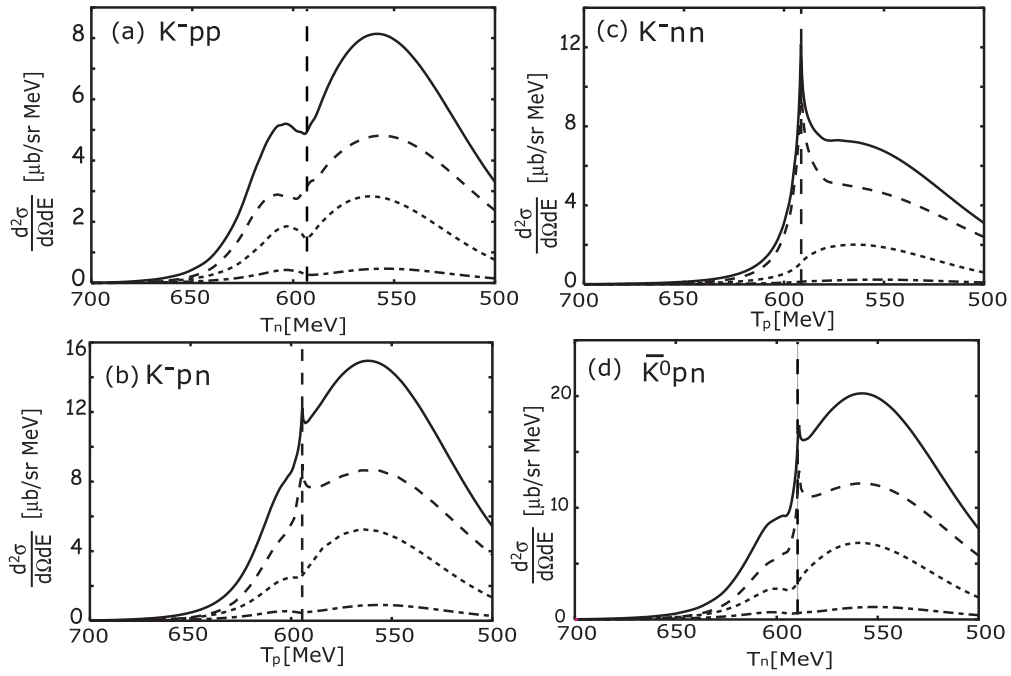

Figure 3: Conversion (kaon absorption) part of formation spectra for (a) ^{3}He(K^-, n)K^-pp [Fig. 2 (a)], (b) ^{3}He(K^-, p)K^-pn [Fig. 2 (c)], (c) $t(K^-, p)K^-nn$ [not discussed in this proposal], and (d) ^{3}He(K^-, n)$\overline{K}^0pn$ [Fig. 2 (b)], as a function of emitted nucleon energy at $T_{K^-} = 600\,\mathrm{MeV}$ ($p_{K^-} = 976\,\mathrm{MeV}/c$). Solid lines correspond to the total conversion spectra. Taken from [34].

Therefore, by assigning the product of $\overline{K}NN$ in the reaction (a–c) to the configuration (1–3), it would be naïvely supposed that reaction (a) is the most favored channel to produce a K^-pp bound state, with some fraction into configuration (3). To the contrary, the other two reactions (b, c) lead to all the configuration (1–3). Koike and Harada estimated the relative production cross section of each configuration by using the transition amplitude of the elementary processes in Table 7 of [36].

Very recently, Yamagata-Sekihara *et al.* obtained the inclusive formation spectrum for each reaction, as shown in Fig. 3 [34]. As expected, a bump structure, corresponding to the K^-pp bound state, is seen in case of ^{3}He(K^-, n)K^-pp reaction (Fig. 2 (a)), and a smaller bump structure is also found in the ^{3}He(K^-, p)K^-pn reaction (Fig. 2 (c)). According to the authors, the spectra (b) and (d) in Fig. 3 resembles each other, because the optical potentials for K^--pn and $\overline{K}^0$-pn were equal due to the isospin symmetry. Some differences between the two spectra are because of distortion, elementary reaction rate, and so on.

Both the theoretical studies [34, 36] stressed the importance of simultaneous measurement of the ^{3}He(K^-, n) and ^{3}He(K^-, p) reactions [3].

In this proposal, we propose to measure the ^{3}He(K^-, p) and ^{3}He(K^-, n) reaction si-

[3]For completeness, ^{3}H(K^-, p)K^-nn reaction is also important since it provides unique information on pure $T = 3/2$ $\overline{K}NN$ state. However, a radioactive tritium target is experimentally unrealistic.

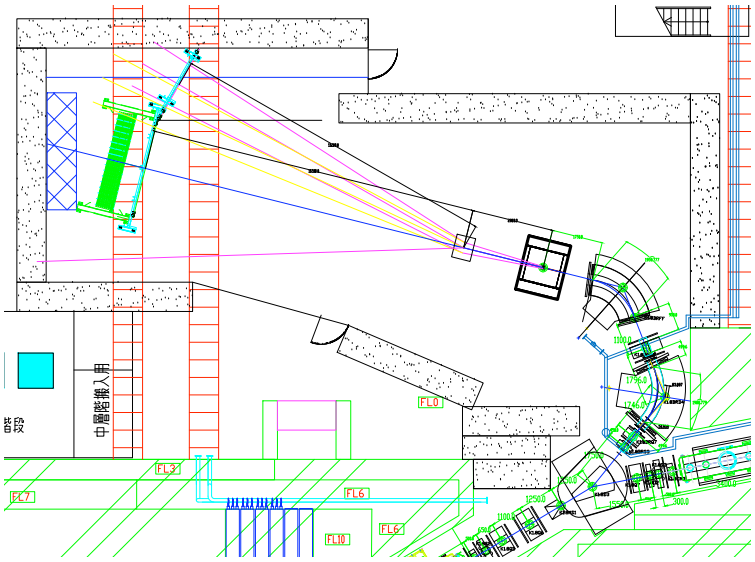

Figure 4: Present layout plan of the E15 experiment. A set of proton TOF counters (cyan) is also drawn in front of the neutron counter (green).

multaneously, by installing an additional "proton detector system" in the original E15 setup. The detail of the system is discussed in the following section.

Not only the semi-inclusive spectra of the (K^-, $nX^\pm$) and (K^-, $pX^\pm$) reactions ($X^\pm$ will be detected by a cylindrical detector system), rich information (PID, momenta, correlation, ...) of decay particles will be available for further analyses by using the cylindrical detector system, compared with the pioneering KEK-PS E548 experiment which equipped NaI detectors as a decay counter. For example, by identifying a Λ via $p+\pi^-$ decay, we may be able to search for a neutral-charged kaon-nuclear bound state K^-pn, from the successive reactions:

$$K^- + {}^3\mathrm{He} \to K^-pn + p \quad , \quad K^-pn \to \Lambda + n$$

in analogy with

$$K^- + {}^3\mathrm{He} \to K^-pp + n \quad , \quad K^-pp \to \Lambda + p$$

which is the objective of the E15 experiment. A neutron, which is not detected by the cylindrical detector system, may be reconstructed by the missing mass of ^{3}He(K^-, $p\Lambda$)X, if the momentum resolution of the scattered proton and is good enough.

2 Experimental setup

2.1 E15 experiment

Figure 4 shows the present layout plan of the K1.8BR area for the E15 experiment. The K1.8BR beamline spectrometer is an SQDQD magnet system, split at the D3 magnet from the K1.8 beamline. The last dipole magnet D5 has been added to bend the beam trajectory further, for the distance between the ^{3}He target and the neutron counter should be as long as 15 m to improve the missing-mass resolution, as requested

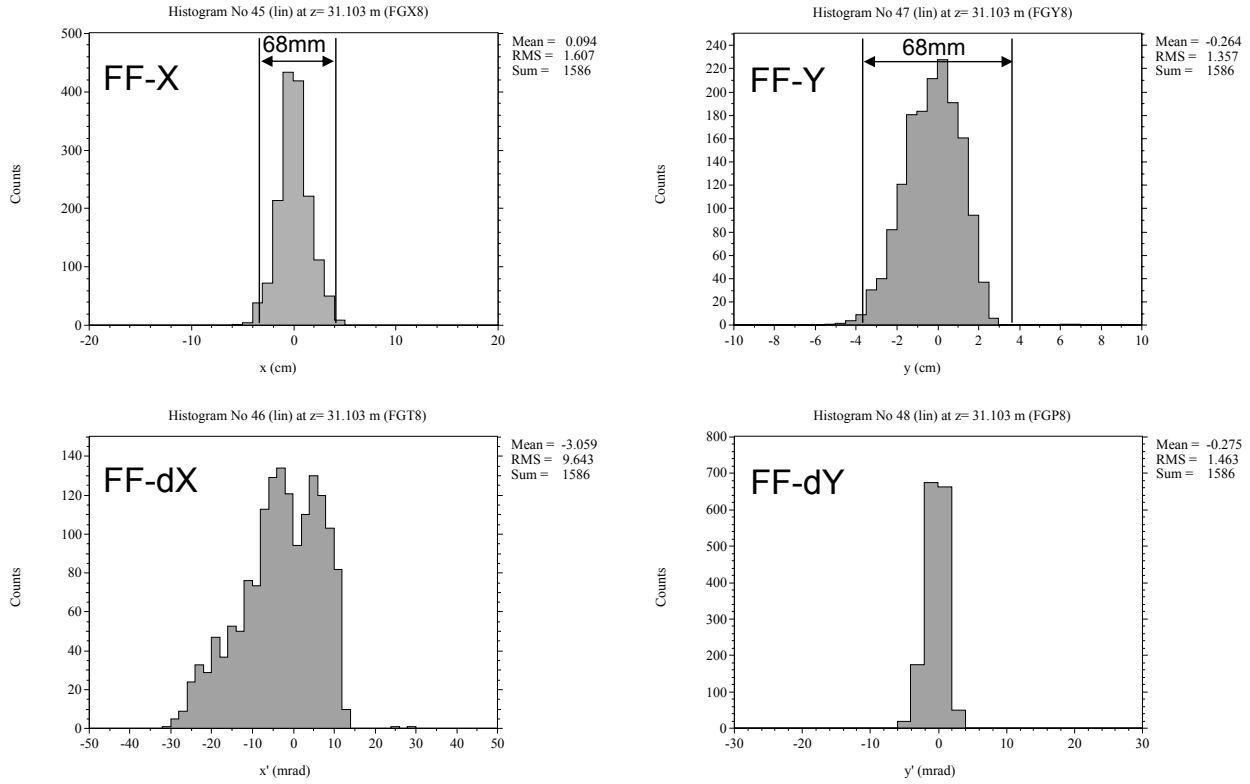

Figure 5: Beam profile at the final focus, calculated by the TURTLE code. The optics is based on the K1.8BR Option 2′.

in the E15 proposal. Figure 5 shows a calculated result of the beam profile at the target position.

A ^{3}He target will be located in the center of a cylindrical detector system (CDS). It consists of a solenoide magnet, a cylindrical drift chamber (CDC) and scintillation counter hodoscopes (CDH). This system will be used for the reconstruction of the decay particle of K^-pp, such as Λ and proton.

The neutron from the ^{3}He(K^-, n) reaction will be detected by a neutron counter (NC), 15 m downstream of the target. It will be composed of 112 scintillation counters (20 cm × 5 cm × 150 cm), and will be arranged as 3.2 m in width (16 segments) and 35 cm in depth (7 layers) [4].

In order to avoid non-interacting beam kaons and their decay particles entering the neutron counter directly, a beam sweeping magnet will be installed around 2.8 m downstream of the target. We have decided to use the USHIWAKA magnet, whose maximum magnetic field is 1.5 Tesla and pole length is 65 cm. The central trajectory after the dipole magnet (set to 1.4 Tesla (0.9 Tesla · m)) is indicated by a purple line, bent toward the left side of the neutron counter.

The detail of each detector system can be found in the E15 proposal [14].

[4]The arrangement has been changed from 14 segments × 8 layers as decribed in the proposal.

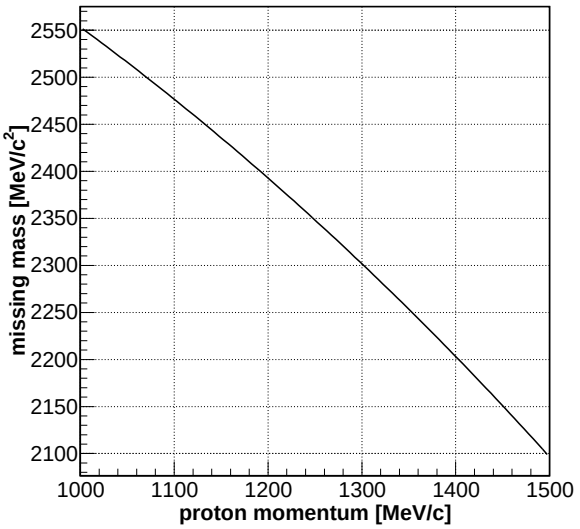

Figure 6: The relationship between the momentum of the proton emitted at zero degree and the missing mass in ^{3}He(K^-, p) reaction.

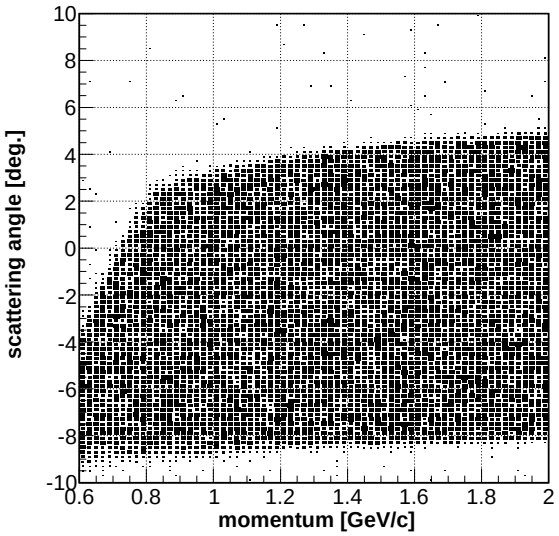

Figure 7: The horizontal acceptance of the pole gap of the beam sweeping magnet, as the function of the momentum of positively charged particles.

2.2 Proton detector system

A proton will be swept out by the beam sweeping magnet in the opposite direction to the beam K^-. The trajectories of 1.0 and 1.4 GeV/c protons with the horizontal scattering angle 0°, ±3° (relative to the beam) are drawn by purple and yellow lines in Fig. 4, respectively.

We are planning to install the following detectors to detect the protons in the momentum range between 1.0 GeV/c and 1.4 GeV/c, which corresponds to the missing mass (binding energy from the $K^- + p + n$ threshold) of 2.55 GeV/c^2 ($B = -180$ MeV) and 2.20 GeV/c^2 ($B = 170$ MeV), respectively. The relationship between the forward proton momentum and the missing mass is depicted in Fig. 6. The momentum acceptance is required to cover not only the bound region but also the unbound region, like the KEK-PS E548 experiment has already measured (see Fig. 1).

1. TOF start counter
2. TOF stop counter
3. Drift chamber
4. Cherenkov counter for proton identification

A schematic view is shown in Fig. 8.

The detection acceptance of protons is mainly restricted by the existence of the dipole magnet, which is also the case for neutrons, but is rather complicated because of the motion of protons in a magnetic field. The vertical acceptance of the system is limited within ±3° which is determined by the pole gap of the dipole magnet and

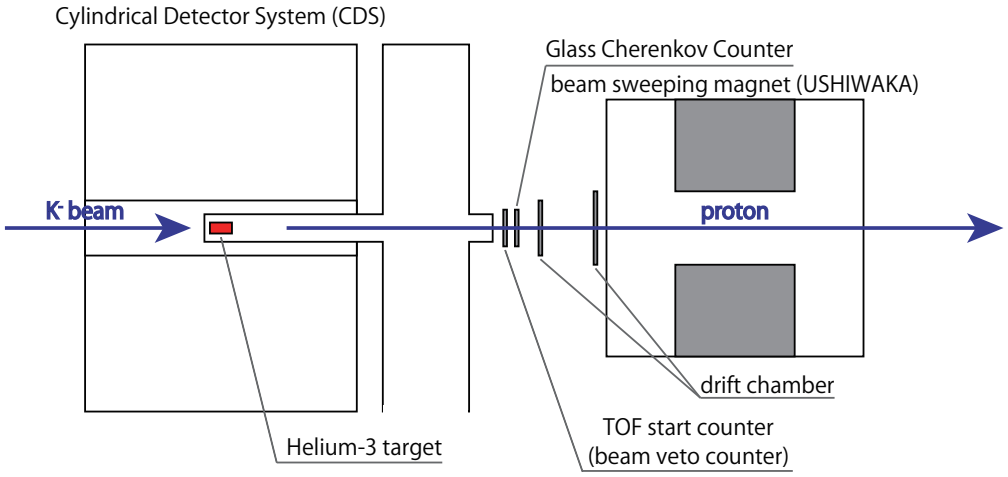

Figure 8: Schematic side view of the proton detector system, together with the cylindrical detector system and the beam sweeping magnet.

the height of the existing TOF stop counters (the same as the neutron scintillation counters). On the other hand, the horizontal acceptance is dependent on the charge and the momentum. Figure 7 shows the requirement to pass through the pole gap. It is asymmetric with respect to the zero-degree line, simply because of the deviation of the trajectory to one side. Instead of momentum-dependent acceptance, we will concentrate on the minimum acceptance of $\pm 3^\circ$ between 1.0 GeV/c and 1.4 GeV/c [5]. This acceptance is just half of that for neutrons (6° in the horizontal direction and 3° in the vertical one). The dimension of each detector to be installed will be determined so as to cover the horizontal/vertical scattering angle within at least 3°.

The velocity of a forward-emitted particle will be measured by the time-of-flight (TOF) between the start and stop counters, which is the same method as for neutrons. The momentum resolution $\Delta p/p$ is shown in Fig. 9, when the TOF resolution is assumed to be $\sigma = 120$ or 150 ps. If the TOF resolution can reach 120 ps, which was the same as assumed for neutrons in the E15 proposal, the momentum resolution will be from 0.95% at 1.0 GeV/c to 1.6% at 1.4 GeV/c. Correspondingly, the missing-mass resolution is estimated as shown in Fig. 10. For example, it will be $\sim$ 19 MeV/c^2 (FWHM) at the threshold (2.37 GeV/c^2), if the TOF resolution is $\sigma = 120$ ps.

Generally, the TOF resolution for protons is expected to be better than that for neutrons; a scintillation counter irradiated by a charged particle can produce a signal immediately after it enters into the counter, while a neutron penetrate into some depth before reacting with hydrogen or other nuclide. The ambiguity on the reaction point worsens the time resolution [6]. Therefore, we expect a slightly better missing-mass

[5] It may be possible to detect a largely scattered proton with $-8^\circ < \theta_x < -3^\circ$, where θ_x is the horizontal scattering angle, by a wide TOF stop counter wall, and then the statistics will be increased by a factor of 3. However, a Cherenkov counter with the total internal reflection method, which will have a strong a dependence on the incident angle of a particle, will be used for trigger purpose. The behavior of the counter for a large incident angle above 3° will be investigated in future.

[6] The standard deviation of the reaction depth, assuming an uniform distribution within the thickness of the counter d, is $d/\sqrt{12}$. Then, the ambiguity of the reaction time is expressed as $d/(\sqrt{12}v)$, where v is the

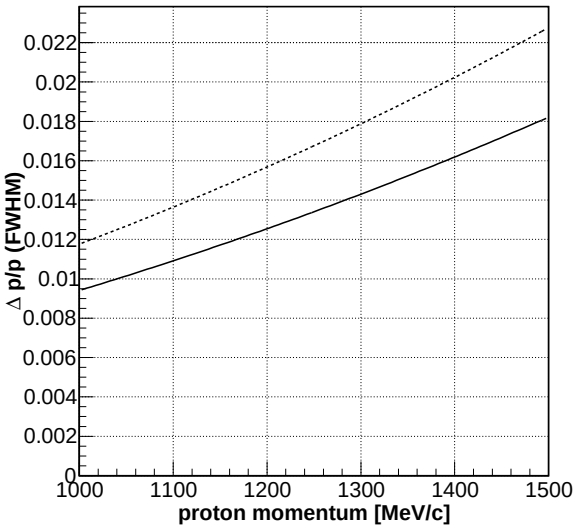

Figure 9: Expected momentum resolution of protons, assuming the TOF resolution of $\sigma = 120\,\mathrm{ps}$ (solid line) and 150 ps (dashed line).

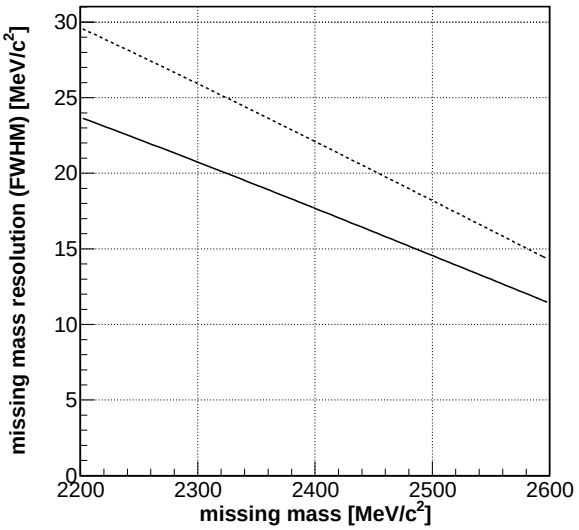

Figure 10: Expected missing-mass resolution, assuming the TOF resolution of $\sigma = 120\,\mathrm{ps}$ (solid line) and 150 ps (dashed line).

resolution will be attained for the (K^-, p) reaction by using the same TOF method.

As for the particle identification of protons from others, the information of velocity obtained from the TOF analysis will be mainly used. First of all, a negative particle, including the beam K^-, will be bent away from the right side of the TOF stop counters, where protons will arrive. If a positive particle with its velocity βc were a π^+ instead of a proton, the momentum should be smaller by a factor of m_π/m_p, where m_π and m_p are the mass of pions and protons, respectively. Then, the region of interest of β (1.0–1.4 GeV/c for protons) corresponds to 150–210 MeV/c for pions. A particle with such a low momentum will never pass through the sweeping magnet, since the radius of the trajectory inside the magnet (1.4 T) is calculated to be below 50 cm, smaller than the pole length.

In addition, two sets of drift chambers will be installed between the cryostat and the beam sweeping magnet, in order to measure the scattering angle of particles emitted from the target. After the velocity of a particle is estimated from the time-of-flight, the track connecting the hit positions of these chambers can be extrapolated, taking into account the bending angle in the sweeping magnet, and it will be checked whether the hit in the TOF stop counter is associated with the track. Here, the particle is assumed to be a proton, for calculating the momentum or the bending angle. If it is actually not a proton, the track will be extrapolated incorrectly, and will not connect to the hit in TOF stop counter. In other words, information on the scattering angle and the hit position the TOF stop counters can be useful to evaluate the bending angle in the

velocity of a particle. For example, it is estimated to be around 60 ps for 1.2 GeV/c neutrons entering into 5 cm-thick neutron counters.

magnet roughly, and the mass of the particle can be calculated.

A Cherenkov counter will be installed between the target and the sweeping magnet on purpose to distinguish protons from other particles, especially the beam kaons, at the trigger level. Without any on-line particle identification, events in which a K^- travels to the downstream without interacting with the helium-3 target or other materials will overwhelm the events we would like to observe, i.e. the (K^-, p) reaction. The hit information of the TOF stop counter is difficult to be used for the first level trigger, because the TOF stop counter is more than 12 m far away from other detectors, and protons takes more $\sim$ 50 ns before arriving at the TOF stop counter. The delay is further increased because of the turn-back signal cable. Therefore, a detector for on-line particle identification is desirable to be located near the target.

2.2.1 TOF start counter

The "beam veto counter", described in the E15 proposal, will be replaced by segmented scintillation counters. This replacement will not cause any problem in the (K^-, n) measurement. In case of the (K^-, n) reaction, this counter will not be fired because the neutron will pass through it. Events which a non-interacting K^- or its decay particle (with non-zero charge) enters into this veto counter will be removed for this purpose.

It will be located just downstream of the helium-3 cryostat system, as in the E15 proposal. The counter is as large as 16 cm $\times$ 16 cm so as to detect the K^- beam spread from the target position (cf. Fig. 5).

We consider to reuse a set of TOF counters in the KEK-PS E549 experiment. The time resolution is expected to be around 80 ps.

2.2.2 TOF stop counter

As drawn in Fig. 4, two walls of TOF stop counters will be built, 14 m downstream of the target. The size of each counter is 10 cm $\times$ 3 cm $\times$ 150 cm, and the central and the other wall (named as *the extended wall*) consist of 34 and 27 segments in line, respectively. The scintillation counters within the central wall in front of the neutron counter serves as the veto counters for neutron detection in the E15 experiment.

Figure 11 shows the correlation between the proton momentum (1.0–2.0 GeV/c [7]) and the counter ID number (named from left to right; No. 1, 2, ..., 34 in the central wall and No. 35, 36, ..., 61 in the extended wall). Most of the protons emitted from the (K^-, p) reaction do not hit this central wall, and the extended wall is needed on the right side of the central one, viewed from the upstream. In order to detect slower protons down to 1.0 GeV/c with its horizontal scattering angle 3°, the width of the extend wall should be as long as 2.1 m.

Therefore, we would like to request at least 2.5 m space to locate the extended wall, next to the central wall.

[7] In this proposal, we don't need to detect a particle above 1.4 GeV/c. However, a proposal to measure deuterons from the ^{3}He(K^-, d) Λ^*(1405) reaction will be submitted [39]. The momentum range of deuterons to be detected is 1.4–1.8 GeV/c. All the detectors except for the Cherenkov counter in the proton detector system will work for deuteron detection with small modification.

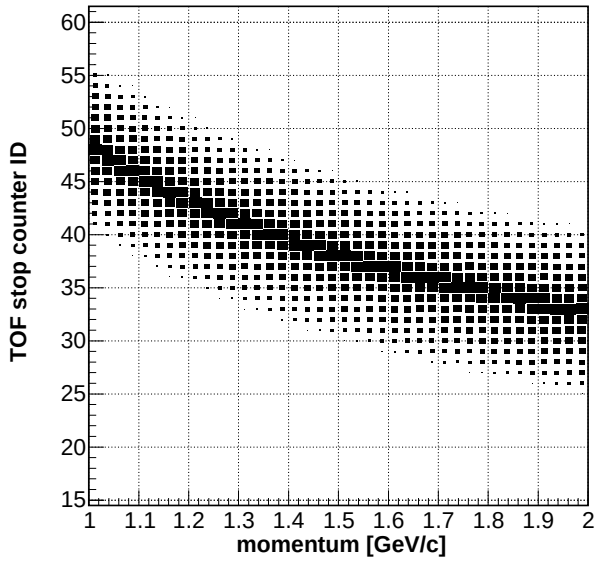

Figure 11: Correlation between proton momentum and irradiated TOF stop counter. The scattering angle is uniformly distributed within 3°.

2.2.3 Drift chamber

The two chambers, upstream of the magnet, will be operated in a high rate condition like those in the beamline, because the non-interacting kaons and their decay particles pass through these chambers before swept out by the dipole magnet. Figure 12 is a rough estimation of the beam profile at 1.7 m downstream of the target, around where a drift chamber is to be installed. Here, the beam profile at the target (see Fig. 5) was approximated to a Gaussian shape, and the trajectories are extrapolated. The beam intensity at the target was assumed to be 1.0 MHz (7×10^5 K^- per spill with 0.7 sec flat top operation). In-flight decay of kaons was not considered. According to this result, two sets of 5 mm-pitched drift chambers with $xx'yy'$ planes will be a possible candidate. Since the scattering angle 3° corresponds to a spread of about 10 cm at this position, drift chambers with sensitive area $> 20\,\text{cm} \times 20\,\text{cm}$ need to be produced [8]. These chambers are also used for measuring the scattering angle precisely.

2.2.4 Cherenkov counter

For the on-line separation between scattered protons from beam kaons, a Cherenkov counter will be employed. The velocities of 0.97–1.03 GeV/c kaons (assuming 3% momentum bite) and 1.0–1.4 GeV/c protons are $\beta = 0.891$–0.902 and $\beta = 0.729$–0.831, respectively. In order to distinguish them, the velocity threshold must be set between 0.831 and 0.891.

One of the candidates is a TIR (total internal reflection) Cherenkov counter with

[8] If a large scattered protons are to be detected as discussed in footnote 5, a larger drift chamber is required.

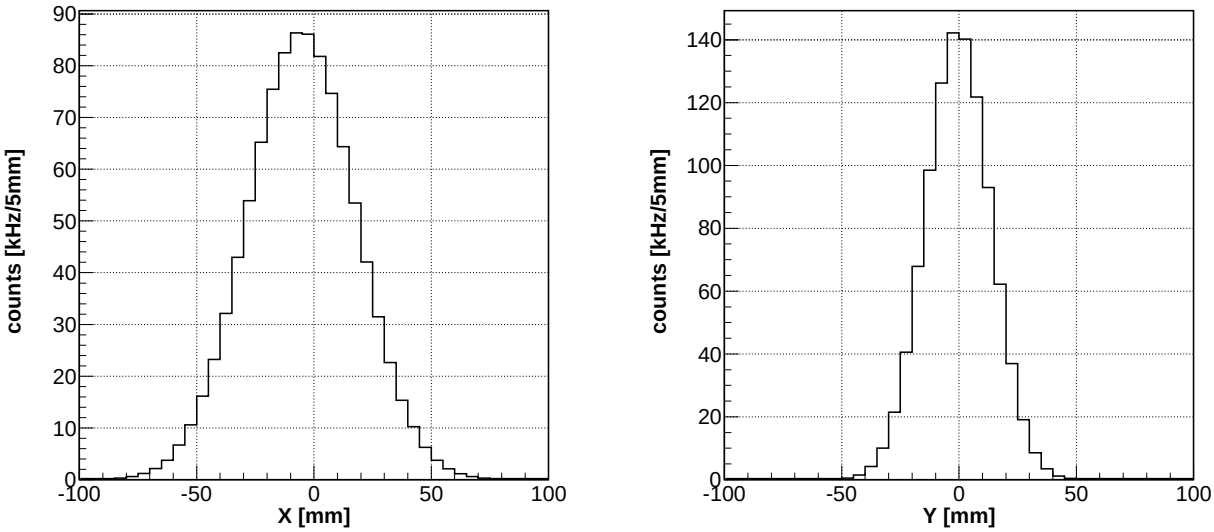

Figure 12: Beam profile at FF+1.7 m, extrapolated from the profile at FF. The beam profile in Fig. 5 is approximated as a Gaussian shape. See text for details.

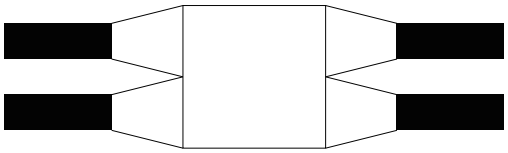

Figure 13: Schematic view of a glass Cherenkov counter.

a borosilicate glass radiator. The TIR threshold for vertically entering particles can be expressed as $\beta_{th} = 1/\sqrt{n^2 - 1}$, where n is the refractive index of the radiator. We plan to adopt Schott BK7 glass [40], whose refractive index is 1.53 at $\lambda = 400\,\mathrm{nm}$. The benefit of using a glass as a radiator is that an excellent accuracy of a plane surface can be achieved with the technique for optical lenses and filters.

The R&D of a glass TIR cherenkov counter is in progress. A schematic view of a counter under design is drawn in Fig. 13. The dimension of the radiator will be $20\,\mathrm{cm} \times 20\,\mathrm{cm} \times 5\,\mathrm{mm}$, large enough to cover the beam size at the counter position. It will be viewed by four PMT's in both side. It should be noted that there are no external reflector such as aluminum foil between the radiator and the light shield, to make use of the TIR condition. The angular dependence of this counter have to be studied carefully because the TIR condition changes for a particle entering with an finite incident angle. The minimal requirement for this counter is that Cherenkov photons *never* enter into PMT's in *both* side, for a proton with an incident angle (which is equal to its scattering angle in principle) less than $3\sqrt{2} \sim 4.5°$. On the other hand, the beam has small angular divergence (see Fig. 5) and a kaon irradiating into the radiator almost vertically is expected to emit a Cherenkov light, some of which will eventually arrive at PMT's in both sides after multiple TIRs.

2.3 Influence to the (K^-, n) measurement

After installation of the proton detector system, a scattered neutron will have to pass through the glass Cherenkov counter and drift chambers, as well as the beam veto counter and the charge veto counter in front of the neutron counter. The latter two are required already for the E15 experiment. The loss of neutrons by the glass Cherenkov counter (1.25 g/cm^2 for 5 mm thickness) is estimated to be $\sim 2\%$ by a simple simulation. The total mass thickness of drift chambers is much smaller than that of the glass radiator, and their contribution can be ignored. Even when the radiator needs more thickness to increase the number of Cherenkov photons, the loss caused by newly installed counters will be controlled not to exceed 10%.

3 Trigger

We consider two kinds of triggers for the (K^-, p) measurement.

- inclusive condition (K^-, p),
- semi-inclusive condition (K^-, $pX^{\pm}$)

where $X^{\pm}$ is a charged particle detected by the cylindrical detector system. When the scattering angle is small ($\lesssim 2^\circ$), the trajectory of an additional particle detected by CDS has to be used to estimate the reaction vertex. The inclusive measurement will be possible only when the scattering angle is large enough and the crossing point of the beam and the scattered proton can be obtained with a sufficient accuracy. The trigger will be prescaled so as not to reduce the DAQ efficiency, since they are mixed with several triggers for the E15 experiment.

For the (K^-, n) reaction, only the semi-inclusive condition and the exclusive condition can be useful, since the trajectory of a neutron can not be analyzed directly. In order to compare two kinds of semi-inclusive spectra (K^-, $nX^{\pm}$) and (K^-, $pX^{\pm}$) with enough statistics, their prescale factors will be close to each other.

4 Beamtime request

The formation cross sections of the (K^-, n) and (K^-, p) reactions are expected to be in the same order (see Fig. 1 or Fig. 3). The detection efficiency is almost 1 for protons, three times more than for neutrons (about 1/3 expected for 35 cm-thick neutron counter), and the geometrical acceptance is about half of that for neutrons, as described in Sec. 2.2. Thus, the detection of a forward proton about 1.5 times more efficient than of a forward neutron.

Since the aim of this proposal is to compare their formation spectra, we consider the beamtime given for the E15 experiment is enough. Therefore, we will not request any more beamtime in this proposal.

5 Schedule

Scintillation counters in the KEK-PS E549 experiment will be reused for the TOF start counters. The TOF stop counters already exists, half of them were used in the E549

Table 1: Cost estimation for the proton detector system.

item	cost (kYen)	budget
TOF start counter	—	existent
TOF stop counter (scintillation counter)	—	existent
TOF stop counter (support)	1,000	not funded
Drift chamber and support	5,000	not funded
glass Cherenkov counter	2,000	Grands-in-Aid
total	8,000	

experiment and the other half will be used for the beam tuning in FY2009. By the end of FY2010, the TOF counter system will be constructed.

The R&D of the glass Cherenkov counter started in FY2008, and will be completed in the middle of FY2010 after some test experiments.

Drift chambers will be newly designed and constructed if a budget request is successfully adopted. They will be ready also in the end of FY2010. In case there is not plenty budget to construct new chambers, a possibility to reuse old chambers might be considered seriously.

The installation of all these counters will be planned to finish in the beginning of FY2011. At the latest, it should be completed not later than the E15 experiment is ready and the (K^-, n) measurement can be started.

6 Cost estimation

The production of the glass Cherenkov counter is supported by the Grants-in-Aid for Young Scientists (2008–2009). At present, there are no budget for drift chambers, and we will apply for budgets such as Grants-in-Aid. The cost estimation is summarized in Table 1.

References

[1] Y. Nogami, Phys. Lett. **7**, 288 (1963).

[2] M. H. Alston *et al.*, Phys. Rev. Lett. **6**, 698 (1961).

[3] Y. Akaishi and T. Yamazaki, Phys. Rev. C **65**, 044005 (2002).

[4] T. Yamazaki and Y. Akaishi, Phys. Lett. **B515**, 70 (2002).

[5] T. Yamazaki and Y. Akaishi, Phys. Rev. C **76**, 045201 (2007).

[6] M. Sato *et al.*, Phys. Lett. **B659**, 107 (2008).

[7] M. Iwasaki *et al.*, arXiv:nucl-ex/0310018.

[8] T. Suzuki *et al.*, Mod. Phys. Lett. A **23**, 2520 (2008).

[9] T. Suzuki *et al.*, Phys. Rev. C **76**, 068202 (2007).

[10] M. Agnello *et al.*, Phys. Rev. Lett. **94**, 212303 (2005).

[11] N. Herrmann, in: A. Hirtl. (Eds.), Proceedings of EXA05, Austrian Academy of Science Press., Vienna, 2005, pp. 73–81.

[12] G. Bendiscioli *et al.*, Nucl. Phys. **A789**, 222 (2007).

[13] T. Yamazaki *et al.*, arXiv:0810. 5182[nucl-ex] (to appear in the Proceedings of EXA08).

[14] M. Iwasaki, T. Nagae *et al.*, J-PARC E15 proposal. http://j-parc.jp/NuclPart/pac_0606/pdf/p15-Iwasaki.pdf

[15] FOPI Collaboration, Experimental proposal to GSI (2007).

[16] AMADEUS Collaboration, Letter of Intent (2006).

[17] Y. Ikeda and T. Sato, Phys. Rev. C **76**, 035203 (2007); Y. Ikeda and T. Sato Phys. Rev. C **79**, 035201 (2009).

[18] N. V. Shevchenko, A. Gal, and J. Mareš, Phys. Rev. Lett. **98**, 082301 (2007); N. V. Shevchenko, A. Gal, J. Mareš, and J. Révai, Phys. Rev. C **76**, 044004 (2008); N. V. Shevchenko and J. Révai, Few Body Syst. **44**, 187 (2008).

[19] A. Doté, T. Hyodo, and W. Weise, Nucl. Phys. **A804**, 197 (2008); A. Doté, T. Hyodo, and W. Weise, Phys. Rev. C **79**, 014003 (2009).

[20] A. Arai, M. Oka, and S. Yasui, Prog. Theor. Phys. **119**, 103 (2008).

[21] E. Friedman and A. Gal, Phys. Rep. **452**, 89 (2007).

[22] E. Friedman, A. Gal and C. J. Batty, Phys. Lett. **B308**, 6 (1993).

[23] E. Friedman, A. Gal and C. J. Batty, Nucl. Phys. **A579**, 518 (1994).

[24] C. J. Batty, E. Friedman and A. Gal, Phys. Rep. **287**, 385 (1997).

[25] A. Ramos and E. Oset, Nucl. Phys. **A671**, 481 (2000).

[26] A. Baca, C. García-Recio, and J. Nieves, Nucl. Phys **A673**, 335 (2000).

[27] T. Kishimoto, Phys. Rev. Lett **83**, 4701 (1999).

[28] A. Cieplý, E. Friedman, A. Gal, and J. Mareš, Nucl. Phys. **A696**, 173 (2001).

[29] K. Ikuta, M. Arima, and K. Masutani, Prog. Theor. Phys. **108**, 917 (2002).

[30] J. Yamagata, H. Nagahiro, Y. Okumura, and S. Hirenzaki, Prog. Theor. Phys. **114**, 301 (2005); Erratum *ibid.* **114**, 905 (2005).

[31] J. Yamagata, H. Nagahiro, and S. Hirenzaki Phys. Rev.C **74**, 014604 (2006); J. Yamagata and S. Hirenzaki, Eur. Phys. J. **A31**, 255 (2007).

[32] T. Kishimoto *et al.*, Nucl. Phys. **A754**, 383c (2005).

[33] T. Kishimoto *et al.*, Prog. Theor. Phys. **118**, 181 (2007).

[34] J. Yamagata-Sekihara, D. Jido, H. Nagahiro, and S. Hirenzaki, arXiv:0812.4359v1 [nucl-th].

[35] T. Koike and T. Harada, Phys. Lett. **B652**, 262 (2007).

[36] T. Koike and T. Harada, Nucl. Phys. **a804**, 231 (2008).

[37] O. Morimatsu and K. Yazaki, Prog. Part. Nucl. Phys. **33**, 679 (1994).

[38] G. P. Gopal *et al.*, Nucl. Phys. **B119**, 362 (1977).

[39] H. Noumi *et al.*, J-PARC proposal (to be submitted for 8th PAC meeting).

[40] SCHOTT AG – optical glass datasheets. (`http://www.schott.com/advanced_optics/english/download/datasheet_all_english.pdf`)